Cu $K^h\alpha_{1,2}$ hypersatellites: Suprathreshold evolution of a hollow-atom x-ray spectrum

R. Diamant,[1] S. Huotari,[2] K. Hämäläinen,[2] C. C. Kao,[3] and M. Deutsch[1]
[1]*Physics Department, Bar-Ilan University, Ramat-Gan 52900, Israel*
[2]*Department of Physics, University of Helsinki, P.O. Box 9, FIN-00014, Helsinki, Finland*
[3]*NSLS, Brookhaven National Laboratory, Upton, New York 11973*
(Received 9 May 2000; published 19 October 2000)

A high-resolution pure Cu $K^h\alpha_{1,2}$ hypersatellite spectrum was measured by photoexcitation using synchrotron radiation. A shift $E(K^h\alpha_2)-E(K\alpha_1)=281.4\pm0.3$ eV from the diagram lines, a splitting $E(K^h\alpha_1)-E(K^h\alpha_2)=23.6\pm0.4$ eV, and an intensity ratio $R=I(K^h\alpha_1)/I(K^h\alpha_2)=0.29\pm0.02$ are found for the two lines of the spectrum. Full-spectrum fits based on *ab initio* Dirac-Fock calculations agree well with the measured spectrum, when QED corrections and Breit interaction are included. A slightly higher calculated R may indicate that the intermediate coupling is not fully accounted for. The intensity's evolution from threshold (measured to be at 18.351 ± 0.015 keV) shows an unexpectedly long saturation range extending up to ~30 keV. The intensity evolution deviates from the Thomas model, which should be valid in the adiabatic, near-threshold regime. The implications of our results for the Z variation of the coupling, correlations, and atomic interactions across the $3d$ transition elements are discussed.

PACS number(s): 32.30.Rj, 32.70.−n, 32.80.Fb

I. INTRODUCTION

Hypersatellite (HS) spectra originate in transitions where the initial state has two vacancies in the same shell. Thus, electronic correlations are strongly reflected in these transitions and the spectra should, in principle, allow their study. HS's involving two K shell vacancies, denoted $K^h\alpha_{1,2}$ and arising from the $1s^{-2}(^1S_0)\rightarrow1s^{-1}2p^{-1}(^{1,3}P_1)$ transitions, are of particular interest for a number of reasons. First, since the initial state requires the excitation of two electrons in the same shell, the spectral characteristics should be affected significantly by, and hence allow studying, *intrashell* correlations. Also, for medium-Z atoms and above the K shell is already significantly relativistic and thus relativistic effects on atomic correlations could be studied using the HS spectra. Moreover, the $K^h\alpha_{1,2}$ HS spectrum consists of two lines $K^h\alpha_1$ and $K^h\alpha_2$, the strengths of which are determined by the coupling scheme dominating the atom. The $K^h\alpha_1$ line originates in the $^1S_0\rightarrow{}^3P_1$ spin flip transition, which is dipole forbidden in the pure LS coupling scheme and allowed only in the intermediate coupling one [1,2]. The intensity ratio $R=I(K^h\alpha_1)/I(K^h\alpha_2)$ therefore depends strongly on the degree of intermediacy of the coupling [3]. This renders the HS the most sensitive (and almost the only) method for quantitatively studying the coupling variation with Z from the LS coupling limit at low Z to the jj coupling limit at high Z. $K^h\alpha_{1,2}$ HS spectra are also unique in allowing study of the Breit-Wigner interaction, the most elusive and least studied of all atomic interactions. Almost all atomic transitions are dominated by the Coulomb interaction and the contribution of the Breit-Wigner interaction amounts to less than 1%. In contrast, for the HS transitions the contributions from the Coulomb interaction to the shift of the $K^h\alpha_{1,2}$ HS lines from the $K\alpha_{1,2}$ diagram lines mostly cancel out, and the contribution of the Breit interaction can reach as high as 20% at high Z [4,5].

Hypersatellites are also the ''diagram'' spectra of *hollow atoms* [6]. This term was coined by Briand *et al.* [7] to describe atoms where a whole inner shell is empty, while the outer shells are occupied. The formation mechanism and properties of such atoms are of fundamental interest to basic atomic physics [6–9]. Hollow atoms are also of great importance for studies of atoms very far from equilibrium and of ultrafast dynamics in atoms, with possible wide-ranging applications in physics, chemistry, biology, and materials science [10]. They have also been proposed as a way of achieving population inversion and lasing for hard x-ray lasers [10,11]. For all of these reasons hollow atoms are currently a very active, and fast-growing, field of research [6]. To date such atoms have been almost exclusively created by electron pickup from metallic [7] or insulating [12] surfaces by highly charged stripped ions traveling close to the surface. The number of electrons picked up and their distribution among the various empty shells of the stripped ion are almost uncontrollable in such experiments. Studies of hollow atoms prepared by the much better controlled single- [9] or multiphoton [13,10] excitation processes are very scarce. The few that are available are either low resolution, or employ coincidence techniques resulting in low statistics and addressing only the excitation cross section.

The reason for the scarcity of high-resolution photoexcited HS spectra is the formidable experimental challenges posed by such measurements. These stem from the very low intrinsic probability of creating the initial two-K-hole states. HS were first detected experimentally by Briand *et al.* [14], employing nuclear K electron capture in a radioactive atom. In the electron capture process, as well as in the internal conversion one, only the first K electron is directly ionized and the second is shaken off through correlations, allowing the study of such effects. However, both processes suffer from low activity of the sample. The Z^{-2} decrease in the K capture probability [15] further reduces the available intensity as Z is increased. Moreover, although the correlation-mediated shake-off process dominates the two-K-hole creation, several competing processes also exist: internal

conversion through the internal Compton effect and internal bremsstrahlung, double internal conversion, etc. [16]. Thus, studies employing nuclear decay processes were able to provide information on the second K electron shake probability P_{KK}, but lack the intensity to allow high-resolution measurements of the HS spectrum itself.

As demonstrated first by Wölfli *et al.* [17] double-K vacancies can be created in heavy-ion–atom collisions with a probability about 100-fold higher than in nuclear decay processes. Heavy-ion collisions are, however, violent events where vacancy creation cannot be controlled to produce only the specific two-hole state. Rather, a range of different numbers of vacancies are produced, so that the resultant HS spectra are strongly contaminated by higher-order spectra. The consequent highly overlapping structure does not allow studying the pure HS spectrum with high resolution [18]. Moreover, it has been demonstrated that the cross section for creating the two-K-hole state in heavy-ion collisions increases in quadrature with the intensity of the impinging ion beam. This indicates that the two K vacancies are generated in two independent, direct single-ionization events [18,19], rather than by a correlation-mediated shake-off following a single-ionization event. Thus, initial state correlation effects are only marginally reflected in HS spectra generated in heavy-atom collisions. Light-ion [18,20] and electron [19,21,22] excitations have also been employed in HS studies, the former suffering from low intensity and the latter from high background due to bremsstrahlung.

For several reasons, single-photon excitation is the method of choice for creating the two-K-hole initial state of HS transitions. As the electron-photon interaction is weak, only one electron is ionized directly while the second K hole is created by intrashell correlations, which allows their study. Since the probability of photoexciting more than two electrons is negligible, and since no bremsstrahlung is generated, pure, low-background HS spectra result. However, the photon energy required for two-K-hole excitation in almost all atoms lies in the x-ray region, where high-intensity lasers are not yet available. Thus, only a handful of photoexcitation studies have been published to date, all but a few of them for low-Z atoms like He [23] and Li [13], and addressing only the creation probability of the two-K-hole state by photoabsorption. The very recent study of Kanter *et al.* [9], published while this paper was being written, is the first to measure a photoexcited HS emission spectrum, that of Mo. This is also the first study to employ synchrotron radiation for photoexciting HS spectra in medium-Z atoms. However, the coincidence method employed and the low resolution of the HS detection did not allow resolution of individual lines. Only the ratio of HS to diagram line intensity was determined in that experiment for a single energy of the photoexciting radiation.

An extremely important feature of the photoexcitation method is the ability to tune the energy of the exciting photons. This allows one in principle to study the evolution of the excited emission spectrum from the energy threshold for creating the initial state, called the ''adiabatic'' regime, to the high-excitation-energy limit, called the ''isothermal'' regime, where the intensity and shape of the emission spectrum saturate. The electronic excitation and deexcitation processes of an atom high above the excitation threshold, in the isothermal regime, are separate and consecutive. They have been successfully studied and accounted for within the standard independent-electron–frozen-core–sudden (IFS) approximation. Near threshold, however, the time required for the ejected electron(s) to leave the atom is comparable to the lifetime of the excited state. Thus, the excitation and the deexcitation processes occur on comparable time scales, merging into a single complex process [24]. The slow, adiabatic kinetics renders electronic correlations highly important in this regime [24–26], invalidating, in principle, the IFS approximation. Because of the highly demanding experimental requirements, as discussed above, no experimental studies of the adiabatic regime were available until very recently even for the rather intense diagram spectra of atoms. The adiabatic regime became accessible to high-accuracy spectral measurements only recently, with the advent of suitable insertion device beamlines at synchrotron sources. These provide intense, well focused, x-ray beams of narrow bandwidth and tunable energy for exciting the various x-ray transitions. The consequent emission radiation requires high-resolution spectrometers for resolving the emission spectra. A few such spectrometers have been installed worldwide, mostly for studying inelastic x-ray scattering. Measurements carried out very recently with such techniques of diagram [27], satellite [28], and (the present study of) hypersatellite [29] spectra in Cu and of satellite spectra in Ge [30] from threshold to saturation indicate that the *shape* of the spectrum may be already saturated as close to the threshold as 50 eV. The *intensity*, however, requires a much longer range to saturate, and its dependence on the excitation energy deviates considerably from the currently prevailing perturbation theoretical predictions [31,32].

The $3d$ transition elements are of particular interest for photoexcited HS spectra measurements. On the experimental side, their thresholds for two-K-hole excitations, up to 20 keV, are still within the energy range accessible to currently operational inelastic-scattering-type beamlines at several synchrotron sources. On the scientific side, the $3d$ transition metals are the region where the coupling varies rapidly with Z from an almost pure LS coupling at the low end, $Z \approx 20$, to the clearly intermediate coupling at the high end, $Z \approx 30$ [33]. It is important to note that the various effects discussed above are reflected in the energy positions, line splitting, and intensity ratios of the individual lines comprising the spectra. To properly address the relevant issues it is therefore imperative to have fully resolved HS spectra of good statistical accuracy. For Cu only one such highly resolved HS spectrum, that of Salem *et al.* [21], is available in the literature to our knowledge, albeit with relatively low statistics. Those measurements were carried out with electron excitation at one energy in the isothermal regime. However, the W $K\alpha_2$ diagram line strongly overlaps the Cu HS spectrum in that measurement so that the extraction of several spectral characteristics either was not possible or resulted in an increased uncertainty.

In view of the scarcity of high-resolution HS spectra for the $3d$ transition elements, and, in particular, the absence of

such measurements in the adiabatic regime for HS's of any element, we have undertaken to measure the HS spectra and their evolution from threshold up for a number of $3d$ transition elements. We aim to determine the characteristics of the HS spectra of these elements with high accuracy, and examine the variation of these properties with Z across this critical transition region in the coupling. We present here the results obtained for the Cu $K^h\alpha_{1,2}$ hypersatellites, and their evolution from threshold up. A few of these results were outlined in a previous short publication [29] and will be discussed here only briefly.

II. EXPERIMENT

A. Introduction

The low intensity of the HS spectra, $\lesssim 10^{-4}$ of that of the diagram lines even at saturation, mandates the use of an intense, energy-tunable x-ray source for exciting the atoms. To record pure, well resolved spectra a spectrometer having high resolution, high throughput, and high signal-to-background ratio is required. A wiggler beamline at a synchrotron source was used to meet the requirements of tunability and high intensity. A Johann-type spectrometer, employing a large-area, spherically bent silicon crystal, operating near back reflection, provided the high resolution and the high throughput. We now briefly describe the experimental setup and procedures, concentrating on the features peculiar to the present measurements. Further details, especially about the beamline and spectrometer, have been published elsewhere [34,28].

B. Experimental setup and measurement procedures

The setup is the same employed in our Cu $K\alpha_{3,4}$ satellite study [28], with differences dictated by the different energies. The wiggler beamline X25 at NSLS, Brookhaven National Laboratory [34] was used. The radiation from the wiggler is focused by a toroidal mirror, followed by a two-bounce Si(111) monochromator. This provides an incident energy resolution of ~ 6 eV, and a flux of $\sim 10^{12}$ photons/sec in a spot size of $\lesssim 1$ mm^2 at the sample. The incident intensity is monitored by an ionization chamber. The sample is a polycrystalline high-purity Cu foil 0.5 mm thick. The Johann-type analyzing spectrometer has a Rowland circle of 1 m diameter on a horizontal plane, and a spherically bent 3-in.-diameter Si(111) crystal, used in the fourth order. The high, $\sim 72°$, Bragg angle at the HS energy provides a resolution of 2.8 eV for the detected radiation [35]. Incidence and detection angles are each fixed at 45° relative to the sample's surface. The consequent 90° between incident and detected radiation effectively eliminates scattered background, because of the high degree of the horizontal linear polarization of the synchrotron radiation. The background is further reduced by using a solid-state Ge detector and a helium-filled beam path from the sample to the detector.

Two types of scans were done. The first, denoted ''inscan'' in the following, scanned the incident energy $E_{\text{excitation}}$ keeping the analyzer energy fixed at a specific energy, e.g., the peak of the $K^h\alpha_2$ line. This allowed a convenient detection of the threshold energy and the evolution of the peak intensity with $E_{\text{excitation}}$. The second, denoted ''outscan,'' scanned the analyzer's energy E_{emission} keeping $E_{\text{excitation}}$ fixed and produced a HS spectrum for a fixed excitation energy. Several additional measurements were also done, such as inscans off the HS peaks and outscans below the threshold. These were employed to determine the backgrounds for the inscans and outscans, respectively.

Finally, we also looked for the correlated hypersatellites (CHS's, see below). These lines should appear at roughly twice the energy of the HS's, i.e., ~ 16.2 keV, and are predicted to be 1000-fold weaker than the HS lines. Here we employed the Si(888) reflection of the analyzer at Bragg angles of $\sim 77.5°$. To obtain the highest possible intensity we moved the two-bounce monochromator out of the beam path and allowed the ''white'' radiation from the mirror to impinge directly on the sample. The heat load of the nonattenuated ''white'' beam is sufficient to burn through the uncooled Cu foil sample in less than 1 sec. Thus, a water-cooled copper block was used as sample in the CHS measurements. Also, since only radiation with $E_{\text{excitation}} \gtrsim 18.5$ keV can create the two-K-hole initial state common to both HS's and CHS's, the useless low-energy radiation was eliminated by a 30-mm-thick graphite absorber. Even so, the graphite block had to be shifted from time to time throughout the measurements to avoid drilling a hole through the block by the beam upon prolonged exposure.

C. Data treatment

The signal-to-background ratio of the raw data varied, of course, with $E_{\text{excitation}}$, due to the rapid HS cross-section variation above threshold (see below). At $E_{\text{excitation}} = 20$ keV it was ~ 1 . The raw data were normalized to the incident beam monitor reading, corrected for its approximately $E_{\text{excitation}}^{-2}$ efficiency dependence. All outscans (inscans) for the same $E_{\text{excitation}}$ (E_{emission}) were then summed to a single spectrum, and the intensities corrected for the energy variation of the absorption in the sample of both the emitted and incident photons [36]. For the outscans the background was determined by moving $E_{\text{excitation}}$ below the threshold and measuring the same E_{emission} range. This data set, which of course did not show any HS line, was corrected as above, and could be fitted very well by a straight line. This line was then used to represent the background. In all cases a slight upshift of a few percent was sufficient to bring it into perfect overlap with the low-intensity ends of the measured (and corrected) HS spectra. It was then subtracted from the corrected spectrum. The data sets obtained after this subtraction were considered to be the background-free, pure HS spectra and were used for the further analysis and the fits described below.

For the inscans, the background was determined by scanning $E_{\text{excitation}}$, with the spectrometer positioned at an E_{emission} value far away from the HS line peaks, i.e., at the low-energy end of the outscan range. This corrected background scan was slightly shifted up to fit the below-threshold intensity in the outscan taken at the $K^h\alpha_2$ peak. It was then

subtracted off, leaving the background-free outscans discussed and fitted below.

D. Energy and intensity calibration

Since the HS threshold energy is ~18.5 keV, the incident energy was calibrated using the absorption edge of niobium [37], $E(\text{Nb } K)=18.9869$ keV. The Cu $K^h\alpha_2$ HS line at ~8330 eV is very close to the W $L\alpha_2$ diagram line. Thus, the spectrometer's energy scale was set by using a tungsten sample to measure the W $L\alpha_{1,2}$ emission spectrum and assigning the known [37] $E(\text{W } L\alpha_2)=8335.2$ eV to the W $L\alpha_2$ peak.

The spectrometer does not allow one to measure directly both the diagram and HS spectra under comparable conditions. Thus, the W $L\alpha_{1,2}$ spectrum, which *is* measurable directly with exactly the same setup as the HS spectrum, was used to obtain a relative intensity scale for the HS spectra. The measured $R_1=I(\text{Cu } K^h\alpha_1)/I(\text{W } L\alpha_1)$ intensity ratio is put on a diagram-relative intensity scale by using the $R_2=I(\text{W } L\alpha_1)/I(\text{Cu } K\alpha_1)$ intensity ratio calculated from published cross sections [38]. The diagram-relative ratio is then obtained as $R_{Int}\equiv I(\text{Cu } K^h\alpha_1)/I(\text{Cu } K\alpha_1)=R_1R_2$.

To determine R_1 the two spectra, measured by outscans under identical conditions except for the different samples, were first corrected for sample absorption of both incident and emitted x rays and their respective linear backgrounds subtracted. The W spectra, where the count rate was high, were also corrected for the dead time of the counting electronics, including the multichannel analyzer used for energy discrimination. The individual lines in each spectra, shown in Figs. 1(a),(c), were then each fitted by a single (Cu) or several (W) Voigt functions, keeping the Gaussian widths of the Voigt function, representing the experimental resolution, fixed at 2.8 eV for all lines and varying each Lorentzian width, height, and position independently. As can be observed from the residuals in Figs. 1(b),(d), the fits are very good, with almost all residuals enclosed within the $\pm 2\sigma$ lines, where σ denotes the standard deviation of the measured points. We note in passing that the W lines each require more than a single Voigt function for a good fit. This may indicate contributions from transitions other than the simple two-line diagram transition $2p_{3/2}^{-1}\rightarrow 3d_{3/2,5/2}^{-1}$ assigned to this spectrum. Relativistic multiconfigurational Dirac-Fock calculations indicate that the full j splitting of the $2p_{3/2}^{-1}\rightarrow 3d_{3/2,5/2}^{-1}$ transitions, comprising many thousands of individual lines (though most of them are very small), need

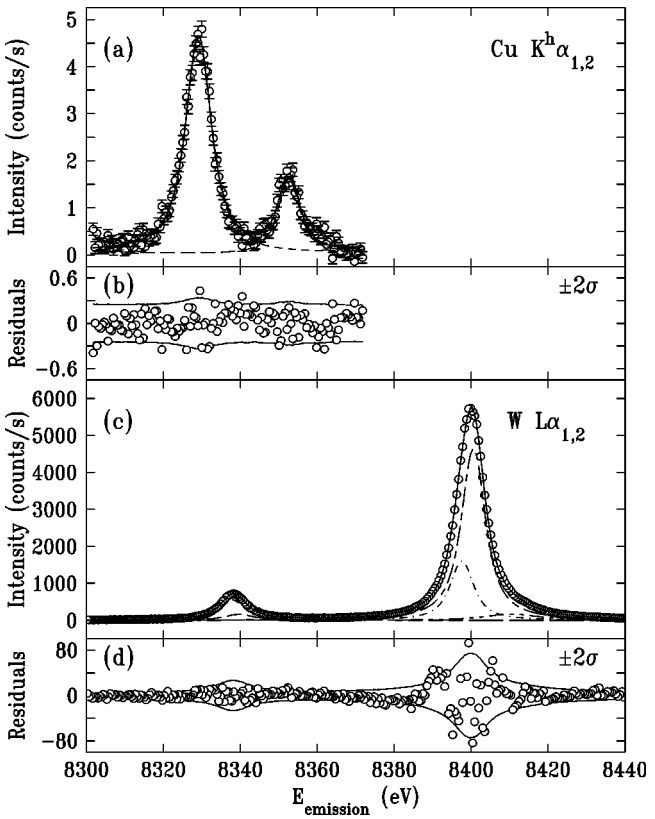

FIG. 1. The measured (points) Cu $K^h\alpha_{1,2}$ hypersatellite (a) and W $L\alpha_{1,2}$ diagram (c) spectra. The lines are fits to a single (a) and several (c) Voigt functions per spectral line. The corresponding fit residuals (b) and (d) (points) are within $\pm 2\sigma$ (lines), where σ is the standard deviation in the measured point, indicating a good fit.

to be taken into account to obtain a good fit to the spectrum [39]. In addition, the W $L\alpha'$ satellite is also found to contribute to the W $L\alpha_1$ line. This satellite has been attributed to the M_3 spectator transition $2p_{3/2}^{-1}3p_{3/2}^{-1}\rightarrow 3p_{3/2}^{-1}3d_{5/2}^{-1}$. However, our measurements, the first high-resolution ones for this line to our knowledge, indicate that the data better support an assignment to the M_5 spectator transition $2p_{3/2}^{-1}3d_{5/2}^{-1}\rightarrow 3d_{5/2}^{-2}$ [40]. The W spectrum is discussed in detail elsewhere [39,40].

R_1 is determined from the areas under the Voigt functions representing the relevant lines. Since the 20 keV excitation energy is far below the W K edge (~70 keV) the W L spectrum is the lowest order one that can be excited. Under these conditions R_2 is given by [41]

$$R_2=[\sigma_{L_3}+\sigma_{L_2}f_{23}+\sigma_{L_1}(f_{13}+f_{12}f_{23})]\omega_{L_3}F_{L\alpha_1}/(\sigma_K\omega_K F_{K\alpha_1}), \quad (1)$$

where σ_i denotes the photoionization cross section of shell i [38], f_{ij} are the probabilities of a Coster-Kronig transition from shell i to shell j [42,43], ω_i is the fluorescence yield of shell i [42,43], and $F_{K\alpha_1}(F_{L\alpha_1})$ is the fraction of the $K\alpha_1$ $(L\alpha_1)$ intensity from the sum of all $K(L)$ x-ray line intensities [44]. Using σ_i, f_{ij}, ω_i, and F values from the indicated references for $E_{\text{excitation}}=20$ keV we obtain $R_2=1.88$. This value was used to calculate the

$I(\text{Cu } K^h\alpha_1)/I(\text{Cu } K\alpha_1)$ intensity scale of the outscans in the discussion below.

An identical method was used for obtaining the relative intensity scale of the inscans. Here the inscans measured with the spectrometer positioned at the emission energies of the Cu $K^h\alpha_2$ and W $L\alpha_2$ peaks were corrected for background, self-absorption, and monitor yield, as above. They were then divided to yield values of R_1 as a function of $E_{\text{excitation}}$. R_2 was calculated at each excitation energy from Eq. (1), interpolating linearly the only $E_{\text{excitation}}$-dependent quantities, the σ_i values of Scofield [38]. The intensity scales obtained in this way for the inscans and outscans closely agree with each other.

The values of $P_{KK}(E)$, the cross section for shake-off/up of the second K electron per single, directly ionized K hole created at a given excitation energy, can be derived from the measured $R_{Int} \equiv I(\text{Cu } K^h\alpha_1)/I(\text{Cu } K\alpha_1)$ discussed above. This is done using

$$P_{KK}(E) = (\omega_K/\omega_{KK})[\mathfrak{I}(\text{Cu K}\alpha_1)/\mathfrak{I}(\text{Cu K}^h\alpha_1)]R_{Int}; \tag{2}$$

where $\mathfrak{I}$ is the fractional intensity of the indicated line compared to the total intensity originating in the corresponding initial state. ω_K/ω_{KK} is the ratio of the fluorescence yields with (ω_{KK}) and without (ω_K) the second K vacancy. This ratio was taken as unity in almost all previous studies. Chen's [33] Dirac-Fock relativistic calculations yield for Cu $\omega_{KK}=0.472$, $\sim 7\%$ larger than [42] $\omega_K=0.44$. The ratio $R_f \equiv \mathfrak{I}(\text{Cu } K\alpha_1)/\mathfrak{I}(\text{Cu } K^h\alpha_1)$ is calculated as

$$R_f = [1 + I(K^h\alpha_2)/I(K^h\alpha_1) + I(K^h\beta_{1,3})/I(K^h\alpha_1)]/[1 + I(K\alpha_2)/I(K\alpha_1) + I(K\beta_{1,3})/I(K\alpha_1)]. \tag{3}$$

Using $I(K^h\alpha_2)/I(K^h\alpha_1)=1/0.29$ (see Table I below), $I(K\alpha_2)/I(K\alpha_1)=0.513$ [38], $I(K\beta_{1,3})/I(K\alpha_1)=0.1839$ [38], and $I(K^h\beta_{1,3})/I(K^h\alpha_1)=I(K\beta_{1,3})/I(K\alpha_1)$ [45], we obtain $R_f=2.76$.

Since the theoretical (and most experimental) P_{KK} values listed in the literature are isothermal regime saturation values, any value measured at a lower energy, like ours at $E_{\text{excitation}}=20$ keV, will have to be scaled up to allow a meaningful comparison. In the absence of a measured $P_{KK}(E)$ curve over the full energy range for any element except the lowest-Z ones, usually (e.g., Ahopelto [46], Keski-Rahkonen [47]) the well-measured He $P_{KK}(E)$ curve is used, scaled by the threshold energy of the element under discussion. We also employ this method, using the recent accurate He $P_{KK}(E)$ measurements of Samson *et al.* [48]. The details are discussed below.

E. *Ab initio* transition calculations

The calculations were done using the relativistic multiconfigurational Dirac-Fock (RMCDF) package GRASP [49], with supplementary code written in house. Previous studies [26,50] indicate that allowing for rearrangement and full relaxation of the excited atom prior to the emission process is important in the isothermal regime. This is done by generating in all cases the initial and final state wave functions in separate, independent runs. The energies of the individual transitions are then obtain by subtracting the appropriate level energies, as calculated in the initial and in the final state runs. This procedure was found to yield accurate energies for the Cu $K\alpha_{3,4}$ satellites even for $E_{\text{excitation}}$ within 50 eV of the threshold [28].

The calculation of relative transition probabilities within each multiplet requires the wave functions of the initial and final states to be orthogonal. Since the initial and final states are generated here in separate runs, this condition is not fulfilled. Thus, as in previous studies [28,50,51], configuration interaction calculations were carried out to obtain the various transition probabilities using once the initial state orbitals and again those of the final state. All the significant transition probabilities in the two sets agreed with each other to within $\pm 10\%$. We used, therefore, the line strengths calculated from the initial state wave functions. This amounts essentially to using the frozen-atom approximation for the line strengths within each multiplet. The implications of this are discussed below. Further details of the calculations are given in Refs. [28,50].

III. RESULTS AND DISCUSSION

A. The emission spectrum

The Cu $K^h\alpha_{1,2}$ spectrum, measured at $E_{\text{excitation}}=20$ keV, corrected for sample absorption and background subtracted as discussed above, is shown in Fig. 1(a). The fit residuals in Fig. 1(b) are within $\pm 2\sigma$ for almost all points, demonstrating a very good fit. Thus, within the measurement's statistics, the intrinsic line shape is well described by the single Lorentzian component of the Voigt function, indicating no contamination by higher-order multivacancy transitions, which invariably plague heavy-ion-excited HS spectra [8,18]. We conclude therefore that photoexcitation yields a pure, intrinsic HS spectrum. The good fit indicates also that the intrinsic HS spectrum does not include contributions from spectator-hole transitions. To merge with the main HS line such transitions must be within less than the half width at half maximum of the HS line's peak energy. This, in turn, requires the spectator hole to be in an outer shell with low binding energy. In a previous experimental study [50], the Cu $K\alpha_{1,2}$ spectrum was shown to include, in addition to the $1s^{-1} \rightarrow 2p^{-1}$ diagram transitions, a $\sim 30\%$ contribution from the $3d-$spectator-hole transitions $(1s3d)^{-1} \rightarrow (2p3d)^{-1}$ and perhaps even a small contribution from the $3p-$spectator-hole transitions $(1s3p)^{-1} \rightarrow (2p3p)^{-1}$.

TABLE I. Comparison of the values obtained from the fit in Fig. 1 with previous theoretical and experimental values. $\Delta = E(K^h\alpha_2) - E(K\alpha_1)$, $\delta = E(K^h\alpha_1) - E(K^h\alpha_2)$, and $R = I(K^h\alpha_1)/I(K^h\alpha_2)$. $\Gamma_{1,2}$ are the full widths of the two lines at half maximum. P_{KK} is the probability of creating a second K hole per direct ionization of a first K electron. The numbers in parentheses are the uncertainties in the last digit of the respective values.

Source	Δ (eV)	δ (eV)	Γ_2 (eV)	Γ_1 (eV)	R	$10^4 P_{KK}$
			Experiment			
Present	281.4(3)	23.6(4)	6.9(8)	5.5(8)	0.29(2)	1.3(3)[a] 3.4[b]
SKS[c]	283.0(30)	21.0(40)			0.27(7)	
B[d]	283.0(30)	23.0				
MCB[e]			5.3(5)			
			Theory			
Present with QED	281.6	23.7			0.32	
Present without QED	288.1	25.4				
CCM[f]	282.2	23.8			0.32	
Å[g]					0.26	
ÅS[h]	280.0	25.6				
MCB[i]			5.7			
Z+1[j]	275.8	23.1				
N[k]	288.0	23.0				
KDKS[l]						5.0
KM[m]						0.88
FSBDD[n]						1.0
MT[o]						0.3

[a]Measured at $E_{\text{excitation}} = 20$ keV.
[b]Scaled to the saturation limit. See text.
[c]Salem, Kumar, and Scott, Ref. [21].
[d]Briand *et al.*, Ref. [1].
[e]Mossé, Chevallier, and Briand, Ref. [20].
[f]Chen, Crasemann, and Mark, Ref. [53].
[g]Åberg *et al.*, Ref. [54].
[h]Åberg and Suvanen, Ref. [74].
[i]MCB's [20] semiempirical formula. See text.
[j]Calculated as discussed in the text.
[k]Nestor. Cited as ''private communication'' by Briand *et al.* [1].
[l]Kanter *et al.*, Ref. [9].
[m]Kornberg and Miraglia, Ref. [58].
[n]Forrey *et al.*, Ref. [59].
[o]Mukoyama and Taniguchi, Ref. [56].

These large spectator-hole contributions account for the skewed line shapes observed for the Cu $K\alpha_{1,2}$ diagram lines [50], and, most probably, also for those of the diagram lines of the other $3d$ transition elements [52]. The ability to fit each of the HS lines measured here by a single Lorentzian component indicates a total absence of such spectator transitions, e.g., $1s^{-2}3d^{-1} \rightarrow 1s^{-1}2p^{-1}3d^{-1}$, in the HS spectra. This is not surprising in view of the very low probability for creating the two-K-hole initial state of the HS transition, and the fact that the spectator states require one additional hole, i.e., a three-vacancy initial state. The vanishingly low probability of exciting such states is responsible, then, for the high purity of photoexcited HS spectra.

The fit in Fig. 1(a) allows us to determine phenomenologically the various characteristics of the measured spectrum without resorting to a specific model for the transition, like the Dirac-Fock calculations discussed below. At the same time the use of Voigt functions allows us to remove the effect of the finite, though small, instrumental resolution. The various quantities obtained from the fit are summarized in Table I, along with values obtained in several previous experimental and theoretical studies. Note that our experimental values in this table, derived using the correct 2.8 eV resolution, differ slightly from those published previously [29], which were calculated using an underestimated 1 eV resolution. The small resultant differences have no significant import on the conclusions of that paper.

Our measured shift $\Delta = E(K^h\alpha_2) - E(K\alpha_1)$ is within ~ 5 eV only of the simple $Z+1$ calculation, using binding energies from Bearden [37] and $\Delta Z \approx 0.57$ and 1 for the

initial *KK* and the final *KL* hole states, respectively, as discussed by Briand *et al.* [1]. Early nonrelativistic Hartree-Fock and Hartree-Fock-Slater calculations [1] overestimate Δ by ~ 30 eV, indicating the importance of relativity here. Nestor's early relativistic Dirac-Fock calculations quoted in [1] are within $\leqslant 10$ eV of the measured values, with the discrepancy assigned to the neglect of correlations [1]. Of the three other relativistic calculations, Chen *et al.*'s [53] and our multiconfigurational relativistic Dirac-Fock ones, which include quantum electrodynamic (QED) corrections, agree better with Δ than does Åberg and Suvanen's [74], which excludes them. The experiment-to-theory differences are well within the errors of previous measurements, which cannot be used therefore to support one calculation over the other. However, when compared to our measurements the calculations deviate by 1σ (our calculation), 3σ (Chen *et al.*), and 5σ (Åberg and Suvanen), clearly indicating that QED corrections are significant. A similar conclusion arises from the splitting, $\delta = E(K^h\alpha_1) - E(K^h\alpha_2)$, where both our results and those of Chen *et al.* are within 1σ of the measured value, while those of Åberg and Suvanen are larger than the measured value by $\sim 5\sigma$. Surprisingly, the $Z+1$ approximated value is also within 1σ of our measured value. The importance of including QED corrections is demonstrated in the significantly larger Δ and δ calculated by us when QED corrections are excluded. The theory deviates from experiment in this case by more than $\gtrsim 20\sigma$ for Δ and $\sim 5\sigma$ for δ, similar to the results of Åberg and Suvanen [74].

As expected, the linewidths $\Gamma_{1,2}$ are about three times larger than the ~ 2.5 eV of the diagram $K\alpha_{1,2}$ lines [50]. The only previously reported width, the Γ_2 of Mossé *et al.* [20], is significantly lower than ours, possibly due to overcorrection for their considerably lower resolution, or their ion-bombardment excitation mode. They suggest a width of $\Gamma_{1,2} = 3\Gamma_K + \Gamma_{L_{2,3}}$ for the hypersatellite lines. Using the *K* and *L* semiempirical level widths $\Gamma_K^{\mathrm{Cu}} \approx 1.5$ eV and $\Gamma_L^{\mathrm{Cu}} \approx 0.5$ eV of Krause [42] yields $\Gamma_{1,2} \approx 5$ eV, somewhat smaller than but in good agreement with the measured value. Additional measurements, however, deviate significantly from this suggestion. For example, this expression yields a width of ~ 0.9 eV for the HS lines of Na, underestimating by more than 50% the 2.2(4) eV measured by Auerhammer *et al.* [19], using electron excitation. For Cu, we use Chen *et al.*'s RMCDF calculated [55] $\Gamma_K^{\mathrm{Cu}} = 1.437$ eV and [33] $\Gamma_{KK}^{\mathrm{Cu}} = 1.77$ eV for the width of the initial *KK* vacancy state. For the final *KL* vacancy state we use the same Γ_K^{Cu} and the $Z+1$ approximated [55] $\Gamma_L^{\mathrm{Zn}} = 0.675$ eV of Zn. The slightly modified Mossé *et al.* approach then yields $\Gamma_{1,2} = (\Gamma_K^{\mathrm{Cu}} + \Gamma_{KK}^{\mathrm{Cu}}) + (\Gamma_K^{\mathrm{Cu}} + \Gamma_L^{\mathrm{Zn}}) = 5.3$ eV, which agrees with our measured Γ_1 but underestimates Γ_2 by $\sim 25\%$. We cannot say at present whether the discrepancy originates in only one or more of the level widths, nor can a source be suggested for the apparent reduction in level lifetimes. High-resolution measurements of the Cu $K^h\beta_{1,3}$ HS spectrum, having the same initial state as but a final state different from the present Cu $K^h\alpha_{1,2}$ spectrum, may shed light on the origin of the deviation from the expected lifetime widths. $K^h\beta_{1,3}$ HS measurements are currently not available for any element.

The two relativistic MCDF calculations, ours and Chen *et al.*'s [53], both overestimate our measured *R* slightly ($\sim 10\%$), albeit by only $\sim 2\sigma$. The simple Hartree-Fock calculation of Åberg *et al.* [54] is surprisingly good, considering that it takes into consideration only the intermediate coupling but no correlations or, of course, QED effects. The good agreement is due, in part, to the use of the measured, rather than the calculated, spin-orbit splitting parameter ζ. The only other extent measurement of *R*, that of Salem *et al.* [21], agrees to within 1σ of their threefold larger error bar with the calculated values. Other nonrelativistic calculations, or those excluding the Breit interaction, yield larger (20–30 %), overestimations [53]. Thus, the intermediate coupling, which dominates this ratio, seems to be mostly accounted for correctly in the RMCDF calculations. However, in the case of *R*, the trend with *Z* is more important than a single value. *R* values of higher- and lower-*Z* elements, measured with an accuracy similar to or better than the present measurements, will be indispensable for elucidating the details of the coupling evolution from *LS* to *jj* across the periodic table. Such measurements are now in progress.

The P_{KK} value derived from our HS $E_{\mathrm{excitation}} = 20$ keV spectrum as detailed in Eqs. (2) and (3) above, is of the right order of magnitude expected from the listed theoretical calculation. Scaling this value (see below) to the isothermal, high-energy regime, where all calculations have been carried out, yields the second value listed in Table I. This value agrees to within $\sim 30\%$ with the empirical prediction of Kanter *et al.* [9], based on their HS measurements for Mo and the He measurements of Samson *et al.* [48]. Considering the difficulties and approximations involved in deriving these values the agreement is very satisfactory. The importance of intrashell correlations is reflected in the tenfold underestimation resulting when these correlations are excluded from the calculations, as demonstrated by the calculations of Mukoyama and Taniguchi [56]. Although it has been suggested that in the isothermal regime such correlations are unimportant [57] both our data and those of Kanter *et al.* indicate that this assumption may be questionable, and that certainly initial state correlations and possibly final state ones as well [56] need to be taken into account. The scaling law approach of Kornberg and Miraglia [58] and Forrey *et al.* [59] circumvents the difficulties of including intrashell correlations in the *ab initio* calculations, and thus reduces the disagreement with experiment by a factor of 2–3. However, as pointed out by Kanter *et al.*, the available data indicate a slower decrease with *Z* than the Z^{-2} predicted by Kornberg and Miraglia. This point is discussed further below.

We have carried out *ab initio* RMCDF calculations of the HS spectrum, using the GRASP code [49] and including QED corrections, as detailed above. The closed $3d$ shell of Cu and the empty *K* shell of the initial state result in a sparse ''stick diagram'' spectrum, shown in Fig. 2(c). Representing each line in this diagram by a Voigt function with a fixed Gaussian resolution width of 2.8 eV, we fitted it to the measured HS spectrum using increasingly fewer constraints. In fit A equal widths were assumed for all lines, and only this width, along with an overall intensity scale factor and a small energy shift (<1 eV) of the calculated spectrum relative to

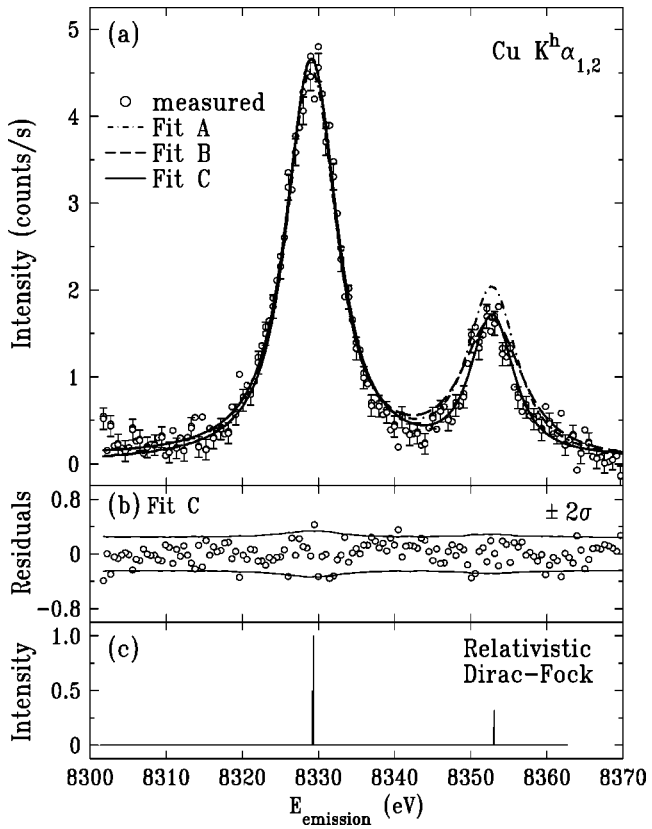

FIG. 2. (a) The measured (points) Cu $K^h\alpha_{1,2}$ hypersatellite spectrum with three progressively less constrained fits (lines) to the calculated stick diagram in (c). See text for details. (b) Residuals of fit C. (c) Multiconfigurational relativistic Dirac-Fock calculated hypersatellite spectrum.

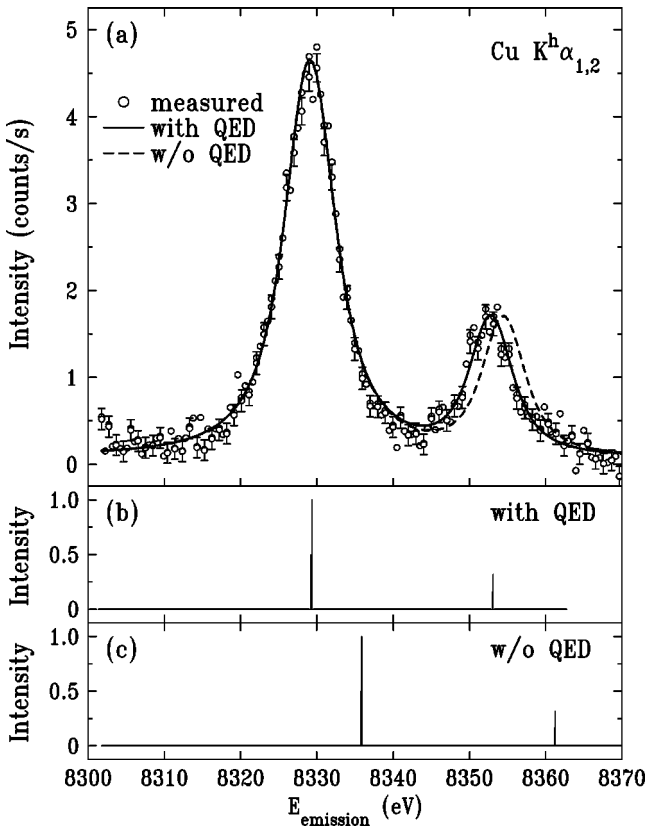

FIG. 3. Measured (points) and theoretical hypersatellite spectra using Dirac-Fock calculations including QED corrections (solid line) (same as fit C in the previous figure) and without QED corrections (dashed line). The corresponding calculated stick diagrams for the two cases are shown in (b) and (c). Note the large shift in the non-QED calculations, and the increased splitting of the two lines, which does not allow a good fit to the measured values even when the shift is eliminated (dashed line). For discussion see text.

the measured one, were allowed to vary in the fit. In particular, the integrated intensity ratio of the two lines was fixed at the calculated ratio, represented by the heights of the respective ''sticks'' in the calculated spectrum. Fit B allows different widths for the two line groups, while fit C allows also the variation of the relative intensity from the calculated values. The energy splitting of the lines is kept fixed at the calculated value in all cases. As can be observed, all three fits agree reasonably well with the measured spectrum. The residuals of fit C, the least constrained and best of the three fits, are shown in Fig. 2(b), and are almost all within $\pm 2\sigma$ of the measured points. The *ab initio* calculated intensity ratio, 0.32, slightly overestimates that of fit C, 0.28. The difference is, however, small: $\sim$15% only. Figure 3 shows what happens when the QED correction is neglected in the RMCDF calculations. As shown in Figs. 3(b),(c) a shift of 7 eV in the positions and an increase of 1.6 eV in the splitting of the lines is obtained. In Fig. 3(a) we plot the measured data (points), fit C (solid line), and the spectrum calculated using the stick diagram calculated without the QED correction (dashed line). The last was calculated using the same Voigt widths as those of fit C, fitting only the shift between the measured and calculated spectra so that the positions of the $K^h\alpha_2$ coincided in both. As can be seen, the incorrect splitting does not allow one to obtain a good fit of the measured spectrum even when the calculated spectrum is shifted to lower energies by the large amount of 7 eV required. Comparing the measured spectrum with more detailed calculations, which include the various components of the QED corrections one at a time, should elucidate the relative importance of each of these contributions.

B. The correlated hypersatellites

Correlated hypersatellite lines originate in simultaneous two-electron–one-photon transitions $1s^{-2}\rightarrow 2s^{-1}2p^{-1}_{1/2,3/2}$, denoted $K^h\alpha_2\alpha_3$ and $K^h\alpha_1\alpha_3$, respectively. Since both HS and CHS spectra originate in the same two-K-hole initial state the branching ratio $B=\sigma(K^h\alpha\alpha)/\sigma(K^h\alpha)$ should be free from effects originating in the excitation process, and allows one to obtain direct experimental information and test theories of the deexcitation process. Several calculations are available for this quantity [60], as well as a number of experimental determinations [61,17,62]. Åberg *et al.* [3] obtained a simple theoretical expression for this quantity as $B_T=[E(K^h\alpha\alpha)/E(K^h\alpha)]^3[D_0(1s2s)]^2$. Here E is the average energy for the transitions indicated and D_0 is the overlap integral, given approximately by $D_0\approx 0.187/Z$. Measurements for Al [61] and Fe and Ni [17,63], as well as more

sophisticated calculations, agree well with the values calculated from this expression. For the $3d$ transition elements the expression above yields values of order 10^{-4}. Salem *et al.* [22,21], however, measured for this branching ratio values of order unity for several $3d$ transition metals. Their study, which employed high-energy electron excitation and a high-resolution, flat crystal spectrometer, is the only non-ion-excited high-resolution measurement of the CHS and HS spectra of the $3d$ transition elements to date. Specifically, for copper, Salem *et al.* measured branching ratios of $\sigma(K^h\alpha_1\alpha_3)/\sigma(K^h\alpha_1)=1.6(3)$ and $\sigma(K^h\alpha_2\alpha_3)/\sigma(K^h\alpha_2)=0.60(25)$. By contrast, the expression above yields $B_T(Cu)\approx 3\times 10^{-4}$, using [21] $E(K^h\alpha\alpha)\approx 16220$ eV and [29] $E(K^h\alpha)\approx 8330$ eV, obtained from the $Z+1$ approximation.

To resolve this discrepancy of four orders of magnitude, we have measured the CHS and HS emission spectra under closely matching conditions. To achieve the highest count rates and best statistics, we removed the incident beam monochromator from the beam path, allowing the mirror-focused beam to impinge directly on the sample. This increased the incident beam intensity by almost two orders of magnitude as compared to the monochromatic intensity obtained at $E_{\text{excitation}}=20$ keV. The configuration of the spectrometer recording the emission spectrum was kept the same except that the analyzer, which was used in the fourth order [i.e., Si(444) reflection] at a Bragg angle $\sim 72°$ for the HS range, was used in the eighth order [i.e., Si(888) reflection] at $\sim 77°$ for scanning the CHS range. The measured CHS range intensity was corrected for the resultant eight-fold lower analyzer reflectivity [64] but otherwise no additional corrections were applied to the two spectra.

The measured spectra are plotted in Fig. 4. The positions obtained for the CHS lines by Salem *et al.* at 16193 ± 10 and 16236 ± 10 eV are marked by arrows on the figure. As can be seen, even though the CHS intensity scale of Fig. 4(b) is enlarged $\sim$20-fold relative to that of the HS scale in Fig. 4(a), no sign of the CHS lines can be found in our measurements. As discussed above, the branching ratio should be independent of the excitation mode of the initial state. Thus, the discrepancy between the present and Salem *et al.*'s results cannot be ascribed to the different excitation mode. We note, however, that the statistics of our measurements impose a limit of $\sigma(K^h\alpha\alpha)/\sigma(K^h\alpha)<10^{-3}$ on the branching ratio, in good agreement with the value obtained from Åberg *et al.*'s [3] expression above. This limit also agrees well with the theoretical values of Gavrila and Hansen [60] of 3.6×10^{-4} and 3.2×10^{-4} for Fe and Ni and the heavy-ion-excited measured values of Stoller *et al.* [62] of $(2.44\pm 0.24)\times 10^{-4}$ and $(2.00\pm 0.24)\times 10^{-4}$ for the same elements.

C. The intensity evolution

Previous measurements [28] of the evolution of the Cu $K\alpha_{3,4}$ satellite complex, originating in $2p^{-1}$ spectator transitions, indicated that the *shape* of the spectrum is evolving only within the first $\sim$50 eV of the threshold, and is unchanged above that. For the present hypersatellites, which

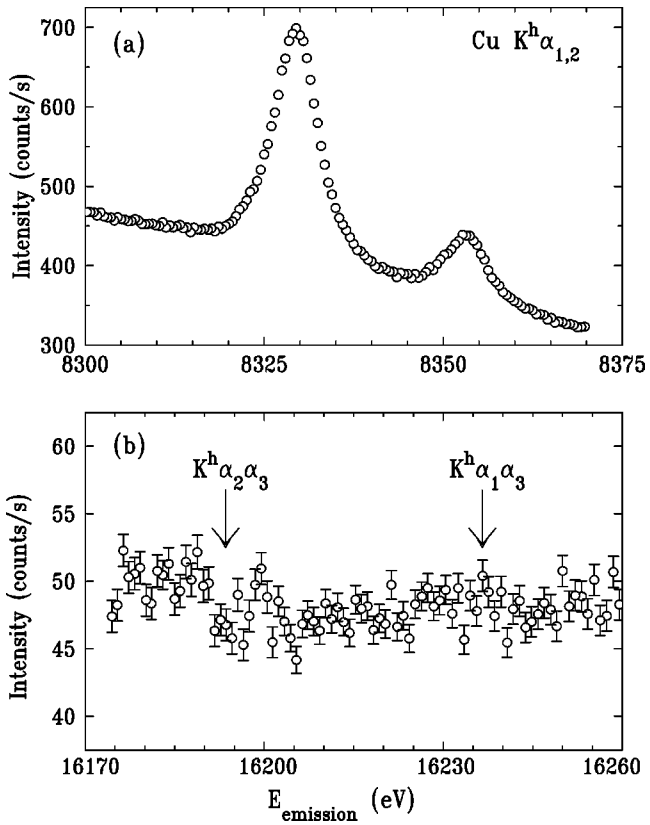

FIG. 4. (a) The ''white''-beam-excited raw Cu $K^h\alpha_{1,2}$ hypersatellite spectrum. (b) The Cu $K\alpha\alpha$ *correlated* hypersatellite energy range, measured under identical conditions. No correlated hypersatellite lines are observed at the expected positions marked.

are, in fact, $1s^{-1}$ spectator transitions, we measured the spectrum at $E_{\text{excitation}}=18.7$, 20, and 23 keV. The first of these, $\sim$350 eV above threshold, is the closest measurement to the threshold allowed by the available incident intensity. Measurements at $E_{\text{excitation}}>23$ keV were out of reach due to the strong decrease in the source's intensity. The measured spectra are shown in Fig. 5, along with fits to a single Voigt function for each line, as discussed above. As can be observed the spectra look very similar at all three excitation energies and the fit-derived parameters agree with each other within their respective errors. We conclude therefore that the shape of the spectrum does not vary significantly for $E_{\text{excitation}}$ higher than $\sim$350 eV above threshold, in agreement with conclusions of the Cu $K\alpha_{3,4}$ satellite study [28]. However, the intensities of the spectra relative to the high-energy, isothermal limit vary considerably in this range. This is shown by the multiplicative scale factors, shown on the figure, that were required to bring the relative intensities to the isothermal limit of 1.

To explore the intensity variation with $E_{\text{excitation}}$, we have positioned the spectrometer at the $K^h\alpha_2$ peak, and scanned the incident beam energy from 17.5 keV up. The resultant $I(K^h\alpha_2)$ vs $E_{\text{excitation}}$ curve, background subtracted and corrected for sample absorption as discussed above, is shown in Fig. 6(a). It seems to saturate at $\sim$23 keV. Note, however, that this curve is proportional to the *total* probability of obtaining the initial two-K-hole state in a neutral atom, not to

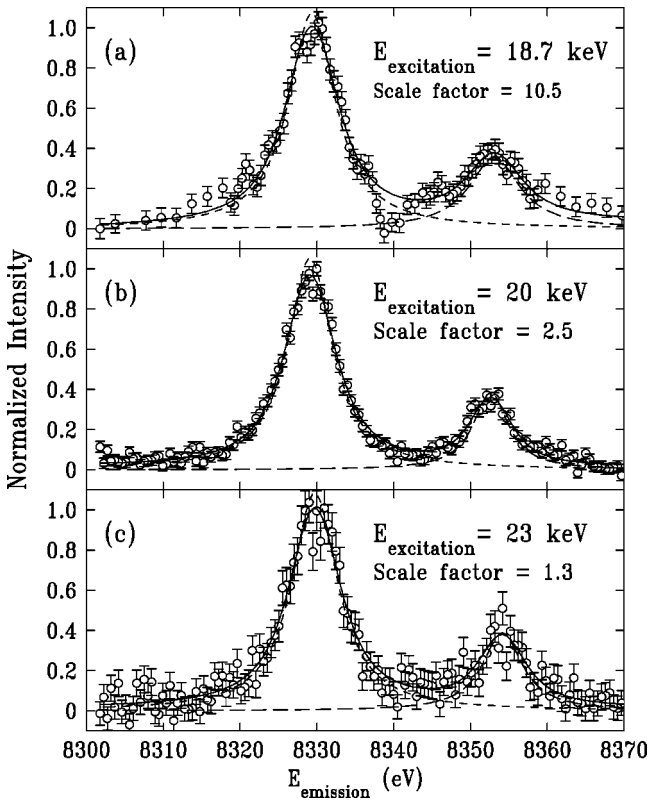

FIG. 5. Measured (points) Cu $K^h\alpha_{1,2}$ hypersatellite spectra excited with monochromatic radiation of the indicated energies, along with a fit, where each line is represented by a single Voigt function (solid line). The individual Lorentzians representing each line with the resolution smearing removed are also shown (dashed lines). No shape variation with excitation energy is observed from (a) $\sim$350 eV above threshold to (c) $\sim$4700 eV above threshold. The multiplicative scale factor required for bringing the relative intensity to the high-energy isothermal limit is also given for each energy. The dip at 8340 eV in (a) is an experimental artifact.

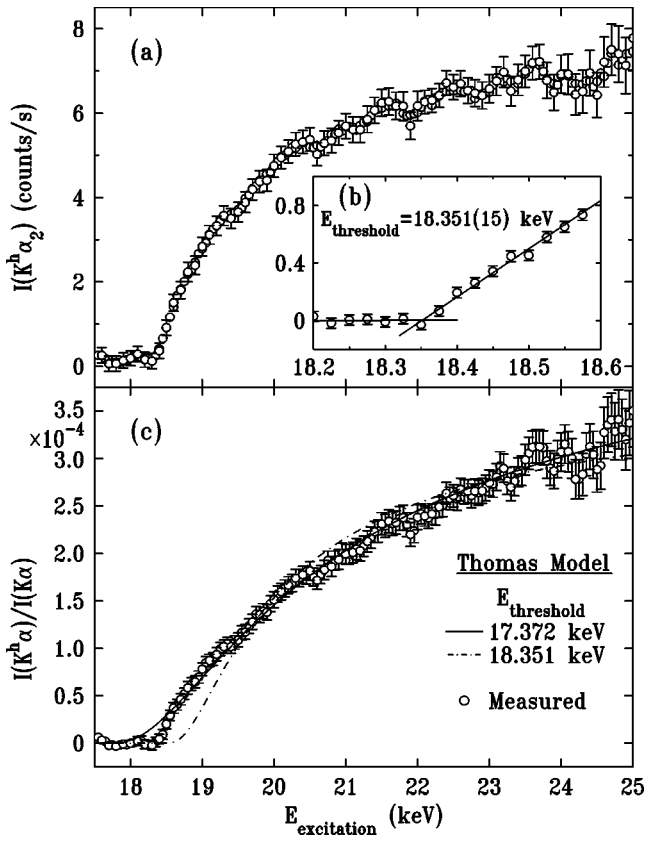

FIG. 6. (a) The intensity variation of the Cu $K\alpha_2^h$ line with incident energy. (b) A finer measurement of the threshold region, yielding the indicated threshold energy. (c) The measured *relative* intensity variation of the hypersatellite spectrum (points), along with the fits to the Thomas model discussed in the text (lines). A four-point ''moving window'' smoothing is used for the data in both (a) and (c) and the fitted models in (c). Note that saturation is not reached even at 25 keV, i.e., $\sim$6.7 keV above threshold.

the probability of obtaining the second K hole per directly ionized first K hole created. To obtain from this curve the $I(\mathrm{HS})/I(\mathrm{diagram})$ ratio, quoted in all other studies, we employed the W $L\alpha_2$ vs $E_{\mathrm{excitation}}$ curve measured under identical conditions, as detailed above for inscans. Figure 6(c) shows the resultant $I(K^h\alpha_{1,2})/I(K\alpha_{1,2})$ (points). A finer scan with better statistics near the threshold, shown in Fig. 6(b), yields $E_{\mathrm{threshold}}=18.352\pm0.015$ keV, in excellent agreement with our $Z+1$ approximated [1] $E_{\mathrm{threshold}}^{Z+1}=18.345$ keV and, to a lesser extent, with our RMCDF calculated [65] $E_{\mathrm{threshold}}^{\mathrm{DF}}=18.378$ keV. As can be observed, even on this magnified scale the intensity rises from threshold smoothly, and no jumps are discernible. According to theory [66], and as demonstrated by the argon Auger satellite measurements of Armen *et al.* [67], the cross section for electron shake-*up* jumps discontinuously at threshold to a significant fraction of its high-energy value. In contrast, the cross section of the shake-*off* process rises smoothly from threshold. The smooth increase shown in Fig. 6(b) implies, therefore, a pure shake-off behavior for the second K hole. This is in line with shake theory's prediction of an increasing shake-off/shake-up ratio with increasing Z and decreasing principal quantum number n of the shaken electron's shell [66,68]. Trends in recent DF calculations for noble gases [68–70] interpolated to the present case of $Z=29$ and $n=1$ predict a contribution of less than 1% from shake-up to the total shake probability. A similarly unobservably low shake-up contribution was also found recently [28] for the Cu $K\alpha_{3,4}$ satellites even though the shake electron originates there in the higher $n=2$ shell. The smooth increase from threshold found for the Ge $K\beta$ satellites in the very recent study of Sternemann *et al.* [30] seems to indicate a pronouncedly shake-off type of behavior even for the $n=3$ shell in that case, although the limits on the shake-up contribution to the measured data are not given there. The error bars of the data in Fig. 6 impose an experimental upper limit of $<3\%$ on shake-up contributions to the HS spectrum at threshold in our case.

The intensity of the Cu $K\alpha_{3,4}$ satellites [28], originating in an $n=2$ spectator-hole transition, was found to saturate at $\sim$1 keV above threshold, which is $\sim$10% of the threshold energy. Here, where the spectrum originates in an $n=1$ spectator-hole transition, saturation is not reached even at the highest energy measured, 25 keV. The discussion in the next section (see Fig. 8 below) indicates that saturation is reached

only around ~ 30 keV, making the saturation range here a surprisingly large ~ 11 keV or almost 60% of the threshold energy. These percentage values, when considered with those of the $n=3$ spectator transitions in Ge [30], where the saturation ranges are $\sim 3\%$ of the threshold energy, indicate a very fast increase in the saturation range with decreasing n of the spectator hole. The Ge measurements, done for $3s^{-1}$, $3p^{-1}$, and $3d^{-1}$ spectator holes, indicate that this range is independent of the orbital quantum number l. Returning now to the satellite and hypersatellite spectra of Cu, we note that both originate in a $1s^{-1}\rightarrow 2p^{-1}$ transition, following a direct photoionization of a single K electron and the shake-off of an additional single electron. The different saturation ranges must, therefore, originate in the different shells of the additional vacancy and the different correlations involved: *KK intrashell* correlations for the hypersatellites and *KL intershell* correlations for the satellites. A better understanding of these trends in the saturation range dependence on n and l of the spectator hole must await detailed adiabatic-regime theoretical calculations, currently not available in the literature.

The measured intensity evolution was fitted to the Thomas model [31,32,71] [Fig. 6(c), lines], which employs time-dependent perturbation theory to describe the shake processes near threshold. This theory accounted well for the measured photoelectron spectra of Ne and Ar [72], although it was found to disagree with the Cu $K\alpha_{3,4}$ satellites [28]. For the Ge $K\beta$ satellites, originating in M shell spectator vacancy transitions, a mixed behavior was found: a reasonable agreement for $3d^{-1}$ spectator satellites, but a poor agreement for $3p^{-1}$ and $3s^{-1}$ spectator satellites [30]. For an error function time dependence of the Hamiltonian (assumed for calculational ease) and a constant velocity of the ejected electron while it is still within the bounds of the atom, the Thomas model yields a closed form expression for the relative intensity:

$$I(K^h\alpha)/I(K\alpha)=I_\infty \exp[-(r^2\Delta E^2)/(15.32\varepsilon)]. \qquad (4)$$

Here r is the radius, in Å, of the shake-off shell, $1s$ in our case. $\varepsilon = E_{\text{excitation}} - E_{\text{threshold}}$ is the excess excitation energy. The binding energy of the shake-up electron, $\Delta E = 9366.3$ eV, is calculated using the $Z+1$ approximation [1] from the Zn K binding energy [37] 9658.6 eV, reduced by 2% as recommended by Parratt [73]. The best fit in Fig. 6(c) (solid line), yields $r=0.024$ Å and $E_{\text{threshold}}^{\text{Thomas}} = 17.372$ keV. While this r is close to our DF calculated [49] 0.028 Å, the calculated curve deviates significantly from the measured values near threshold. Also, the fitted $E_{\text{threshold}}$ underestimates the measured one by ~ 1 keV. Fixing $E_{\text{threshold}}$ at the measured 18.352 keV (dot-dashed line) yields even larger deviations from the measured values near threshold, and a significantly lower $r=0.016$ Å. Similar discrepancies were found for Cu $K\alpha_{3,4}$ satellites [28]. It is possible that a different functional form for the time dependence of the Hamiltonian may yield a better agreement at the cost of having to solve the relevant equation numerically [31,32].

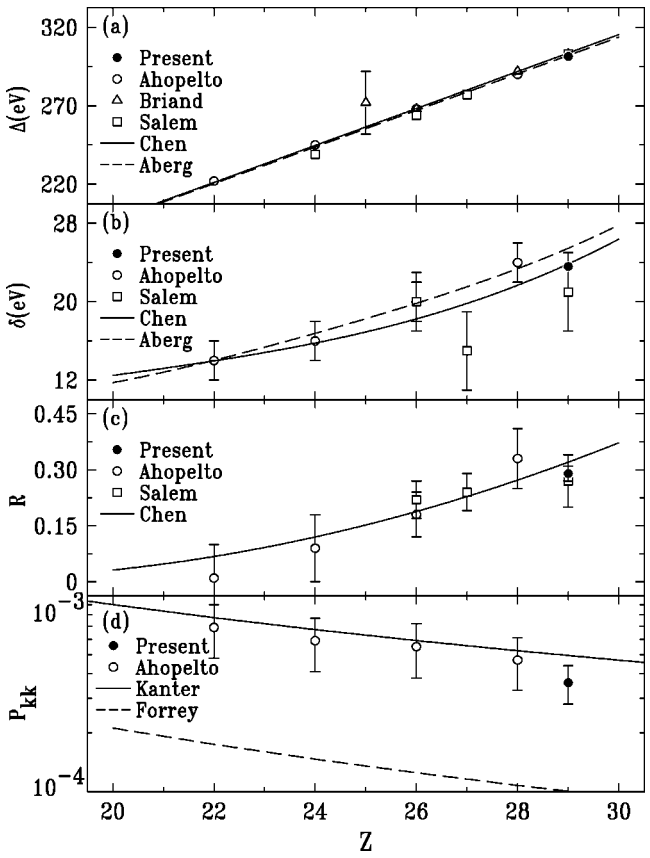

FIG. 7. The variation of the various characteristics of the hypersatellites across the $3d$ transition element range. (a) The shift $\Delta = E(K^h\alpha_2) - E(K\alpha_1)$, (b) the splitting $\delta = E(K^h\alpha_2) - E(K^h\alpha_1)$, (c) the intensity ratio $R = I(K^h\alpha_1)/I(K^h\alpha_2)$, and (d) the probability for creating an additional K hole per directly ionized single-K-hole creation. Points are measured values and lines theoretical and semiempirical calculations. Where error bars are not seen, they are smaller than the symbol size.

D. *Z*-dependent trends

We now compare the values derived above to previous measurements on the $3d$ transition elements. As the various quantities may depend on the excitation mode, as discussed in the Introduction above, we restrict our attention here to experimental studies employing photo- or electron excitation only. Such studies are very few: the pioneering electron excitation study of Briand *et al.* [1] limited to the $K\alpha_2^h$ energies, the low-resolution but relatively comprehensive study of Ahopelto *et al.* [46], measured with Mo $K\alpha$ photoexcitation at a single $E_{\text{excitation}}=17.5$ keV, and the electron-excited high-resolution study of Salem *et al.* [22,21].

The previous and present studies are summarized in Fig. 7, along with several theoretical and semiempirical predictions. As can be observed in Fig. 7(a), within the errors cited, all measured Δ agree well with both theories, since both take into account the relativity, which has a major effect on Δ. Neglecting QED corrections and the Breit interaction in the mixing calculation by Åberg and Suvanen [74] has only a small influence on Δ in this Z range, as discussed above. A much more prominent effect due to this neglect is observed on the splitting δ, shown in Fig. 7(b). Ahopelto *et al.*'s val-

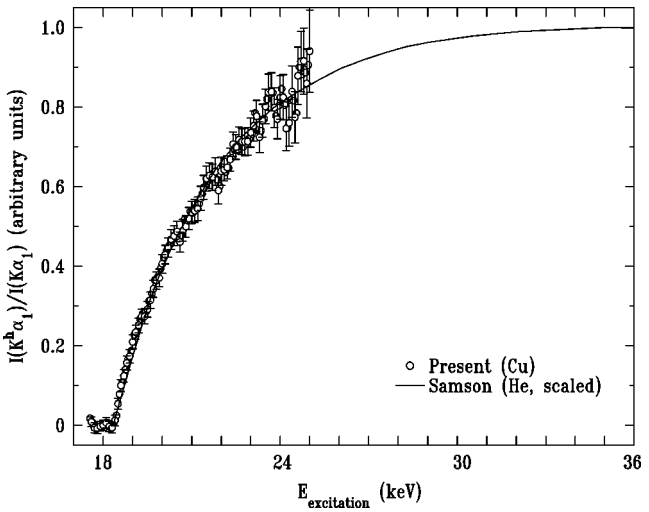

FIG. 8. The high-energy limit scaling of the measured (points) relative hypersatellite intensity, using the He measurements of Samson *et al.* [48] (line). For details see text.

ues cannot distinguish between the two theoretical calculations. Salem *et al.*'s three values either agree (Fe) or are within 2σ of both theoretical values. Our value for Cu agrees very well, within 1σ, with Chen *et al.*'s, while Åberg and Suvanen's overestimates ours by 5σ, as shown also in Table I.

Chen *et al.*'s calculated intensity ratio of the two HS lines is in good agreement with both Ahopelto *et al.*'s and Salem *et al.*'s measured values, as can be observed in Fig. 7(c), indicating that the intermediate coupling is mostly accounted for properly in the calculations. Our measured value seems to yield a somewhat lower value, although the difference is still within 2σ. Finding out whether or not this indicates a real deviation between theory and experiment due to some hitherto unaccounted for effect will have to await measurements with accuracy comparable to ours for both lower- and higher-Z elements.

The values of P_{KK}, the cross section for creating an additional K hole per directly ionized single K hole, is shown in Fig. 7(d). Ahopelto *et al.* scaled their values, measured at $E_{\text{excitation}}=17.5$ keV, to the sudden, high-energy limit using the theoretical $P_{KK}(E)$ curve of Brown [75]. Our P_{KK} value was obtained by a somewhat different method. We used the high-accuracy $P_{KK}(E)$ curve measured by Samson *et al.* [48] for He, and scaled linearly both the energy and P_{KK} axes to fit best our measured $I(K^h\alpha)/I(K\alpha)$ curve over the energy range measured by us, as shown in Fig. 8. We then used this curve to scale our $P_{KK}(E_{\text{excitation}}=20$ keV) value, obtained from our measurements through Eqs. (2) and (3), to the saturation limit. To comply with the practice of Ahopelto *et al.* and other authors we assumed $\omega_K=\omega_{KK}$ for our data shown in Fig. 7(d).

Both the values of Ahopelto *et al.* and ours seem to be in good agreement with Kanter *et al.*'s [9] recent semiempirical $P_{KK}\sim 1/Z^{1.61}$ dependence on Z (solid line), derived from their photoexcited Mo measurements, which employ coincidence techniques to measure P_{KK} directly. The $P_{KK}\sim 1/Z^2$ (dashed line) predicted by shake theory [9] as well as the scaling approach [58,59] for double photoionization of He-like ions underestimate the measured values by almost one order of magnitude. One should, however, bear in mind that with the $\sim 10\%$ reduction in our values and those of Ahopelto *et al.* due to approximating $\omega_K/\omega_{KK}=1$, and the uncertainties involved in the scaling of the measured values to the saturation limit, the theory-experiment agreement, or lack thereof, should not be taken too strictly.

IV. CONCLUSION

We have shown here how the well-resolved, clean Cu $K^h\alpha_{1,2}$ hypersatellite spectrum measured by photoexcitation allows us to address fundamental questions related to intrashell electronic correlations, the transition from LS to jj coupling, the Breit interaction, etc. A comparison of the theoretical and experimental δ, Γ, Δ, R, and P_{KK} indicates the importance of relativity, QED, and the Breit interaction. The measured values obtained for R, and the P_{KK} value derived therefrom, indicate that some discrepancy may still remain between theory and experiment. The evolution of the spectrum's intensity from threshold shows an unexpectedly large saturation range, and distinct trends are identified in its dependence on the primary and orbital quantum numbers. To the best of our knowledge, these trends have not been addressed hitherto by theory. A typical shake-off behavior with smoothly increasing intensity from threshold is found, in agreement with shake theory predictions and previous satellite measurements. The Thomas model does not agree well with the measured intensity evolution, as also found for satellites. A more sophisticated theoretical treatment is clearly called for. HS measurements for neighboring $3d$ transition elements, now in progress, will hopefully shed more light on the remaining discrepancies and, in particular, on the coupling variation with Z. We also hope that the measurements presented here, and the ones now in progress, will stimulate theoretical studies of the various effects and subjects discussed in the present paper, and, in particular, the x-ray emission process in hollow atoms, the adiabatic-regime behavior, and the intrashell correlations in relativistic shells.

ACKNOWLEDGMENTS

This work was supported in part by The Israel Science Foundation, Jerusalem (M.D.) and the Academy of Finland under Grant Nos. 7379/40732 (K.H. and S.H.). Beam time at X25, NSLS, and the assistance of O. Gang in the measurements and of R. Sharon in the data analysis are gratefully acknowledged. Brookhaven National Laboratory is supported by the U.S. Department of Energy under Contract No. DE-AC02-76CH00016.

[1] J.P. Briand *et al.*, Phys. Rev. Lett. **27**, 777 (1971); J. Phys. B **9**, 1055 (1976).

[2] N. Cue, W. Scholz, and A. Li-Scholz, Phys. Lett. **63A**, 54 (1977).

[3] T. Åberg, K.A. Jamison, and P. Richard, Phys. Rev. Lett. **37**, 63 (1976).

[4] J.P. Desclaux, B. Briancon, J.P. Thibault, and R.J. Walker, Phys. Rev. Lett. **32**, 447 (1974).

[5] *Atomic Inner-Shell Physics*, edited by B. Crasemann (Plenum, New York, 1986); B. Crasemann, M.H. Chen, and H. Mark, J. Opt. Soc. Am. B **1**, 224 (1984).

[6] H. Winter and F. Aumayr, J. Phys. B **32**, R39 (1999); H.L. Zhou *et al.*, Phys. Rev. A **59**, 462 (1999); H. Khemliche *et al.*, Phys. Rev. Lett. **81**, 1219 (1998); Y. Azuma *et al.*, *ibid.* **74**, 3768 (1995).

[7] J.P. Briand *et al.*, Phys. Rev. Lett. **65**, 159 (1990).

[8] J.A. Tanis *et al.*, Phys. Rev. Lett. **83**, 1131 (1999).

[9] E.P. Kanter *et al.*, Phys. Rev. Lett. **83**, 508 (1999).

[10] K. Moribayashi, A. Sasaki, and T. Tajima, Phys. Rev. A **58**, 2007 (1998).

[11] K. Moribayashi *et al.*, in *X-Ray Lasers 1998: Proceedings of the 6th International Conference on X-ray Lasers*, edited by Y. Kato, IOP Conf. Proc. No. 159 (Institute of Physics, London, 1999), p. 321; K. Moribayashi, A. Sasaki, and T. Tajima, Phys. Rev. A **59**, 2732 (1999); I. Hughes, Phys. World **8**, 43 (1995).

[12] J.P. Briand *et al.*, Phys. Rev. Lett. **77**, 1452 (1996).

[13] L.M. Kiernan *et al.*, Phys. Rev. Lett. **72**, 2359 (1994).

[14] J.P. Briand, P. Chevallier, M. Tavernier, and J.P. Rozet, Phys. Rev. Lett. **27**, 777 (1971).

[15] A. Migdal, J. Phys. (Moscow) **4**, 449 (1941); E.L. Feinberg, *ibid.* **4**, 423 (1941).

[16] V. Horvat and K. Ilakovac, Phys. Rev. A **31**, 1543 (1985); K. Ilakovec, M. Veskević, V. Horvat, and S. Kaučić, *ibid.* **42**, 3984 (1990).

[17] W. Wölfli, Ch. Stoller, G. Bonani, M. Suter, and M. Stöckli, Phys. Rev. Lett. **35**, 656 (1975).

[18] B. Boschung *et al.*, Phys. Rev. A **51**, 3650 (1995).

[19] J. Auerhammer, H. Genz, G. Kilgus, A. Kumar and A. Richter, Phys. Rev. A **35**, 4505 (1987).

[20] J.P. Mossé, P. Chevallier, and J.P. Briand, Z. Phys. A **322**, 207 (1985).

[21] S.I. Salem, A. Kumar, and B.L. Scott, Phys. Rev. A **29**, 2634 (1984).

[22] S.I. Salem, A. Kumar, B.L. Scott, and R.D. Ayers, Phys. Rev. Lett. **49**, 1240 (1982).

[23] R.P. Madden and K. Codling, Phys. Rev. Lett. **10**, 516 (1963); M. Domke, G. Remmers, and G. Kaindel, *ibid.* **69**, 1633 (1992); O.D. Scwarzkopf, B. Krassig, J. Elmiger, and V. Schmidt, *ibid.* **70**, 3008 (1993).

[24] M.A. MacDonald *et al.*, Phys. Rev. A **51**, 3598 (1995); B. Crasemann, J. Phys. (Paris), Colloq. **48**, C9-389 (1987); V. Schmidt, Rep. Prog. Phys. **55**, 1483 (1992).

[25] J.P. Briand *et al.*, Phys. Rev. A **23**, 39 (1981).

[26] J.W. Cooper, Phys. Rev. A **38**, 3417 (1988); H.P. Saha, *ibid.* **42**, 6507 (1990); M.H. Chen, in *Atomic Inner-Shell Physics* (Ref. [5]).

[27] M. Deutsch *et al.* (unpublished).

[28] M. Deutsch, O. Gang, K. Hämäläinen, and C.C. Kao, Phys. Rev. Lett. **76**, 2424 (1996); M. Fritsch *et al.*, Phys. Rev. A **57**, 1686 (1998).

[29] R. Diamant, S. Huotari, K. Hämäläinen, C.C. Kao, and M. Deutsch, Phys. Rev. Lett. **84**, 3278 (2000).

[30] C. Sternemann, A. Kaprolat, M.H. Krisch, and W. Schülke, Phys. Rev. A **61**, 020501 (2000).

[31] T.D. Thomas, Phys. Rev. Lett. **52**, 417 (1984).

[32] T.D. Thomas, J. Electron Spectrosc. Relat. Phenom. **40**, 259 (1986).

[33] M.H. Chen, Phys. Rev. A **44**, 239 (1991).

[34] K. Hämäläinen, D.P. Siddons, J.B. Hastings, and L.E. Berman, Phys. Rev. Lett. **67**, 8850 (1991); C.C. Kao, W.A. Caliebe, J.B. Hastings, K. Hämäläinen, and M.H. Krisch, Rev. Sci. Instrum. **67**, 1 (1996); K. Hämäläinen, M. Krisch, C.C. Kao, W. Caliebe, and J.B. Hastings, *ibid.* **66**, 1699 (1995).

[35] With a width of $w \approx 1$ mm for the incident beam's focus at the sample, an analyzer/sample distance of $L = 95$ cm, an energy $E = 8330$ eV, and a Bragg angle of $\theta_B = 72°$, the calculated resolution [34] $\delta E = Ew/(L \tan \theta_B) = 2.8$ eV. The same value was obtained by employing a ray tracing program for the experimental setup, from the source to the detector.

[36] E. P. Bertin, *Introduction to X-Ray Spectrometric Analysis* (Plenum, New York, 1978), p. 373.

[37] J.A. Bearden, Rev. Mod. Phys. **31**, 78 (1967).

[38] J.H. Scofield, Lawrence Livermore National Laboratory Report No. UCRL-51326, 1973 (unpublished).

[39] R. Diamant, S. Huotari, K. Hämäläinen, C.C. Kao, and M. Deutsch (unpublished).

[40] R. Diamant, S. Huotari, K. Hämäläinen, C.C. Kao, R. Sharon, and M. Deutsch, J. Phys. B **33**, L649 (2000).

[41] M. Ertuğrul, J. Phys. B **28**, 4037 (1995); D.V. Rao, G.E. Gigante, and R. Cesareo, Phys. Scr. **47**, 765 (1993).

[42] M.O. Krause, J. Phys. Chem. Ref. Data **8**, 307 (1979); M.O. Krause and J.H. Oliver, *ibid.* **8**, 329 (1979).

[43] J.H. Hubbell *et al.*, J. Phys. Chem. Ref. Data **23**, 339 (1994).

[44] N. Broll, X-Ray Spectrom. **15**, 271 (1986).

[45] J.P. Briand, P. Chevallier, A. Johnson, J.P. Rozet, M. Tavernier, and A. Touati, Phys. Fenn. **9**, 409 (1974).

[46] J. Ahopelto, E. Rantavuori, and O. Keski-Rahkonen, Phys. Scr. **20**, 71 (1979); J. Saijonmaa and O. Keski-Rahkonen, *ibid.* **17**, 451 (1978).

[47] O. Keski-Rahkonen, J. Saijonmaa, M. Suvanen, and A. Servomaa, Phys. Scr. **16**, 105 (1979).

[48] J.A.R. Samson *et al.*, Phys. Rev. A **57**, 1906 (1998).

[49] K.G. Dyall *et al.*, Comput. Phys. Commun. **55**, 425 (1989).

[50] M. Deutsch, G. Hölzer, J. Härtwig, J. Wolf, M. Fritsch, and E. Förster, Phys. Rev. A **51**, 283 (1995).

[51] D.F. Anagnostopoulos, R. Sharon, D. Gotta, and M. Deutsch, Phys. Rev. A **60**, 2018 (1999).

[52] G. Hölzer, M. Fritsch, M. Deutsch, J. Härtwig, and E. Förster, Phys. Rev. A **56**, 4554 (1997).

[53] M.H. Chen, B. Crasemann, and H. Mark, Phys. Rev. A **25**, 391 (1982).

[54] T. Åberg *et al.*, J. Phys. A **9**, 2815 (1976).

[55] S.T. Perkins, D.E. Cullen, M.H. Chen, J.H. Hubbell, J. Rathkopf, and J. Scofield, Lawrence Livermore National Laboratory Report No. UCRL-50400, Vol. 30, 1991 (unpublished). See also M. Deutsch *et al.*, Phys. Rev. A **52**, 3661 (1995).

[56] T. Mukoyama and K. Taniguchi, Phys. Rev. A **36**, 693 (1987).

[57] T.A. Carlson and C.W. Nestor, Phys. Rev. A **8**, 2887 (1973).

[58] M.A. Kornberg and J.E. Miraglia, Phys. Rev. A **49**, 5120 (1994).

[59] R.C. Forrey, H.R. Sadeghpour, J.D. Baker, J.D. Morgan III, and A. Delgrano, Phys. Rev. A **51**, 2112 (1995).

[60] T.K. Mukherjee and P.K. Mukherjee, Z. Phys. D: At. Mol. Clusters **42**, 29 (1997); M. Gavrila and J.E. Hansen, J. Phys. B **11**, 1353 (1978); H.P. Kelly, Phys. Rev. Lett. **37**, 386 (1976); A.R. Knudson, K.W. Hill, P.G. Burkhalter, and D.J. Nagel, *ibid.* **37**, 679 (1976).

[61] J. Auerhammer, H. Genz, A. Kumar, and A. Richter, Phys. Rev. A **38**, 688 (1988).

[62] Ch. Stoller *et al.*, Phys. Rev. A **15**, 990 (1977).

[63] W. Wölfli *et al.*, in *Proceedings of the 2nd International Conference on Inner-Shell Ionization Phenomena*, Freiburg, 1976 edited by W. Melhorn and R. Brenn (Freiburg, 1976), p. 272.

[64] R. W. James, *The Optical Principles of the Diffraction of X-Rays* (Ox Bow, Woodbridge, 1982), p. 59.

[65] The energy difference between a neutral, ground state Cu atom and one with two *K* holes, calculated in separate GRASP runs [49], including QED corrections.

[66] T. Åberg, in *Proceedings of the International Conference on Inner-Shell Ionization Phenomena and Future Applications*, edited by R.W. Fink, S.T. Manson, J.M. Palms, and P.V. Rao, U.S. AEC Report No. CONF-720404 (NTIS, U.S. Dept. of Commerce, Springfield, VA, 1972), p. 1509; J. Tulkki and T. Åberg, J. Phys. B **18**, L489 (1985); J. Tulkki *et al.*, Z. Phys. D: At., Mol. Clusters **5**, 241 (1987).

[67] G.B. Armen *et al.*, Phys. Rev. Lett. **54**, 182 (1985).

[68] T. Mukoyama and Y. Ito, Nucl. Instrum. Methods Phys. Res. B **87**, 26 (1994).

[69] D.L. Wark *et al.*, Phys. Rev. Lett. **67**, 2291 (1991); S.J. Schaphorst *et al.*, Phys. Rev. A **47**, 1953 (1993).

[70] T. Mukoyama and K. Taniguchi, Bull. Inst. Chem. Res., Kyoto Univ. **70**, 1 (1992).

[71] E. Vatai, Phys. Rev. A **38**, 3777 (1988); Acta Phys. Hung. **65**, 257 (1989).

[72] F. Heiser, S.B. Whitefield, J. Viefhaus, U. Becker, P.A. Heimann, and D.A. Shirley, J. Phys. B **27**, 19 (1994).

[73] L.G. Parratt, Phys. Rev. **50**, 1 (1936); H.J. Edwards and J.I. Langford, J. Appl. Crystallogr. **4**, 43 (1971); L.G. Parratt, Phys. Rev. **49**, 132 (1936); **49**, 502 (1936).

[74] T. Åberg and M. Suvanen, in *Advances in X-Ray Spectroscopy*, edited by C. Bonnelle and C. Mande (Pergamon, New York, 1980).

[75] R.L. Brown, Phys. Rev. A **1**, 586 (1970).